

Impervious Surface Prediction in Marrakech City using Artificial Neural Network

Sulaiman Mahyoub¹, Hassan Rhinane², Mehdi Mansour³, Abdelhamid Fadil⁴, Waban Al okaishi⁵

Laboratory Geosciences (of Department of Geology) Faculty of Sciences, Hassan II University, Casablanca, Morocco^{1,2,3}

Hassania School of Public Works, Casablanca, Morocco⁴

Laboratory LTI Lab, Faculty of Sciences Ben M'sik, Hassan II University, Casablanca, Morocco⁵

Abstract—Determining an impervious surface is one of the most important topics of remote sensing because of its great role in providing information that benefits decision-makers in urban planning, sustainable development goals, and environmental protection. In recent years, a great development in this field has occurred due to the huge improvement in the algorithms and techniques that are used to map impervious surfaces. In this paper, the deep learning technique has been implemented to investigate the extraction of impervious surfaces in Marrakesh city, based on Landsat images. 9000 polygons and 13840 points have been taken to prepare label data by random forest in Google Earth Engine (GEE). In addition, all preprocessing steps for remote sensing images have been implemented in GEE. An artificial neural network (ANN) has been used to determine impervious surfaces. After training and testing the proposed network on Landsat image datasets, precision, accuracy, recall, and F1-score matrix scores were 0.79, 0.98, 0.87, and 0.82, respectively. The experimental results show that this method is efficient and precise for mapping the impervious surfaces of Marrakesh city.

Keywords—Deep-learning; remote sensing; artificial neural network ANN; impervious surface

I. INTRODUCTION

Impervious surfaces are a prominent indicator of human presence and are characterized as land covers that have been contained by manmade structures that restrict water penetration into the soil, such as building roofs, roadways, and parking lots [1]. The growth of impervious surfaces and urban areas causes a variety of problems, including environmental risks and sociopolitical consequences [2, 3]. In order to achieve sustainable development goals, urban planning, and environmental protection, it is necessary to provide all details and specific information that cover the long-term dynamics of impervious surfaces [4, 5]. Since the 1970s, remote sensing instruments have been widely employed to monitor the Earth. Everywhere across the world, day or night, these satellites gather data at a low cost or for free. With this, the quantity of data that can be used to research impervious surfaces has increased significantly [6-8]. In order to successfully extract information from such a massive volume of data, high-performance processing skills, such as machine learning and cloud computing platforms, are required. These algorithms and technologies have been shown to be extremely efficient [9-12].

Remote sensing has been widely utilized to identify impervious surfaces. Several articles have been published describing the state-of-the-art of this topic [13-21]. Earlier,

statistical remote sensing indices including the Normalized Difference Built-up Index (NDBI) [22], Normalized Difference Impervious Surface Index (NDISI) [23], modified NDISI [24], and perpendicular impervious surface index (PISI) [25], biophysical composition index (BCI) [26], and the normalized difference vegetation index (NDVI) have been developed to map impervious surfaces. Scholars and researchers have moved their focus to machine learning techniques such as Random Forest [27], Support Vector Machine (SVM) [28], and Classification and regression trees (Cart) [29], among others. Similar to our earlier study, this is a continuation of that work [30]. In recent years, deep learning algorithms and cloud computing infrastructures have witnessed tremendous development, resulting in significant advancements in image processing applications such as classification, segmentation, and change detection [31-33]. As a result, the remote sensing community is attempting to modernize remote sensing image preprocessing and processing in order to keep up with this development.

One of these major accomplishments is the Google Earth Engine cloud computing platform, which is free and combines a multi-petabyte catalog of satellite imagery and geospatial datasets with planetary-scale analysis capabilities, as well as its community [34, 35]. This is constantly updated and has many scientists, researchers, and developers working on it to develop remote sensing and environmental applications. Despite the fact that deep learning has unique automatic feature learning capabilities and strong nonlinear complex function expression and fitting capabilities, and it can combine low-level features to form more abstract high-level representations and attribute categories or features, it requires significantly more training data than conventional machine learning supervised classifications [36].

In this work, deep learning techniques have been proposed to determine impervious surfaces of Marrakesh city, based on Landsat images to take advantage of the large archive owned by this satellite (1972–now) [37, 38]. 6787 polygons have been extracted from the cadastral plan, and 13122 labeled points have been chosen carefully from high resolution images to prepare label data images by random forest in the Google Earth engine (GEE). In addition, all preprocessing for remote sensing images for training and testing images has been implemented in GEE. An artificial neural network (ANN) has been used to implement this task. The remainder of this paper is organized as follows: Section II discusses the pieces that are related to this topic. The proposed methodology for predicting

impervious surfaces for the city of Marrakech has been illustrated in Section III. Section IV describes the experimental results and their evaluations. The conclusion is found in Section V.

II. RELATED WORK

In general, the literature on remote sensing techniques for detecting impervious surfaces is divided into three categories: statistical-index based, machine learning based.

1) *Statistical-index based*: In this subsection, index-methods will be discussed briefly. These statistical indicators have been modeled by calculating two or more bands in order to improve the spectrum of specific features of the target areas, such as NDBI, modified NDISI, NDIS, PISI, and BCI. The computing formulas for some of these indicators are presented below:

$$NDBI = \frac{SWIR1 - NIR}{SWIR1 + NIR}$$

$$MNDWI = \frac{G - SWIR1}{G + SWIR1}$$

$$NDISI = \frac{Tb + (MNDWI + NIR + SWIR1)/3}{Tb - (MNDWI + NIR + SWIR1)/3}$$

$$PISI = 0.8192 * B - 0.5735 * NIR + 0.075$$

$$NDVI = \frac{NIR - RED}{NIR + RED}$$

where:

- SWIR1 is the band of shortwave infrared waves (Landsat 8 band 6).while.
- Tb indicated to the temperature of the TIRS1 thermal band's brightness.
- NIR refers to the near-infrared band pixel values (Landsat 8 band 5).
- RED, G, and B represent the red, green and blue canals on Landsat 8, also known as Bands 4, 3 and 2 respectively.

Despite these statistical-based algorithms being obvious and simple to use, they faced a few restrictions in their performance. For example, in regions with large concentrations of topsoil, NDBI does not work well because it cannot distinguish between urbanized areas and vegetation. On the other hand, the NDISI relied on land-surface temperature, which might fail in zones where the heat island effect is less prominent. Furthermore, the Tb band is also problematic since it is not present in all sensors. In general, it's hard to use these indicators alone to predict the impervious surface because the threshold interval changes from zone to zone and hasn't been adjusted yet [25].

a) *Texture-based methods*: Previously, scholars and researchers have extracted the impervious surface using various methods based on spectral analysis and mixed pixel decomposition to examine the variations in reflectance

features of impervious surface areas using medium-to-low-resolution remote sensing images, such as Landsat [39, 40].

b) *Machine learning based*: Machine learning algorithms have been extensively conducted to model impervious surfaces, such as the maximum likelihood classifier, support vector machines (SVM), classification and regression trees (CART) algorithm, and random forest. In spite of the fast development of these approaches, they need vast quantities of labeled training and assessment data. Nonetheless, the gathering and generation of this quantity of labeling data by visual interpretation is regarded as time-consuming and cost-intensive [28]. In addition, the machine learning approach has been challenged by the spectral and textural complexity of impervious surface area (ISA) in mixed pixels, including different combinations of ISA and other land cover types [41].

III. RESEARCH METHODOLOGY

Marrakesh is one of the most important Moroccan cities, it is located at 31° 37' 48" N 8° 0' 32" W, and has a surface area of more than 230 km²; It suffers from the effects of migration from the surrounding countryside to it; it was chosen by the atlas project (www.atlasofurbanexpansion.org/) to study urban expansion from 1985 to the present; and it was also chosen in our previous work [30]. This paper will determine the impervious surface of Marrakesh city using deep learning technique.

A. Database Preparation for Learning and Testing the Proposed Model

Cloud computing is very important for deep learning applications since it provides unlimited storage, provisioning, and updating, as well as guaranteed privacy and security [42, 43]. Users of cloud services can also improve server usage, dynamic scalability, and reduce the time for creating new applications [44]. The Google Earth engine platform (GEE) is utilized to implement all steps for training and testing the deep learning model.

In this study, our goal is to use deep learning techniques to extract the impervious surface of the city of Marrakech based on Landsat images. 6787 polygons and 13122 points have been chosen to prepare labeling data by using random forest in GEE. These points had been collected using visual interpretation analysis, which is based on our power to match patterns and colors in an image to real-world features, from high resolution images from different resources such as (Google earth, Sentinel-2 OSM). According to the polygons, they were taken from plan cadastral of Marrakesh city. Then these data are uploaded to GEE cloud platform as a form of features collections. After that, a sampling operation was performed to link the features (Landsat image datasets 8 bands: B2, B3, B4, B5, B6, B7, NDVI, and NDBI of each point and polygon with the corresponding pixels in the target image (Marrakesh city image).

In the present study, random forest algorithm has utilized to produce labeled data image as it is the best obtained result in our previous study [30]. Fig. 1 shows the resulted image from

random forest, the white pixels represent the impervious surface of Marrakesh city.

Random forest is composed of many decision trees. Furthermore, it employs randomness to improve accuracy and avoid over fitting, which can be a significant problem for such a complex algorithm. These methods generate decision trees from a random sampling of data and extract predictions from each tree. Following that, they vote on the most possible solution. The use of random forest (RF) for image classification has gained popularity due to its ease of use (e.g. relatively insensitive to classification parameters) and generally high accuracy [45]. This algorithm works as follows: Assuming the dataset has "m" features, the random forest will select "k" features randomly, where $k < m$. The algorithm will now select the node with the biggest information gain among the k features as the root node. The algorithm then divides the node into child nodes and continues the procedure "n" times more; a forest with n trees is obtained. Finally, bootstrapping, which entails combining the outcomes of all of the decision trees in random forest, will be performed. Because it is based on the functionality of decision trees, it is definitely one of the most complicated algorithms[46].

After obtaining our labeled image, it is necessary to prepare the database (the labeled image) to be the input of the ANN model. The steps for preparing the database are as follows:

- First step is to flattening the data shape from multi-dimensions (Landsat image datasets eight layers: b2, b3, b4, b5, b7, NDVI, NDBI) into two dimensions array. This is a very important step because Flatten makes the serialization of a multidimensional tensor apparent (typically the input one here eight layers). The mapping between the (flattened) input tensor and the first hidden layer is now possible. Each member of the (serialized) input tensor will be linked with each element of the hidden array if the first hidden layer is "dense". The way the input tensor is mapped into the first hidden layer would be unclear if you didn't utilize Flatten. Fig. 2 shows the result of the flattening operation.
- The second step is data cleaning, by removing no-data pixels from the arrays.
- The third is to divide the data by 60 percent for training and 40 percent for validation accordingly.
- The fourth stage is normalization, which is required by many machine learning methods, including NNs. This indicates that the histogram has been stretched and scaled to meet a particular range of values (here, 0 to 1). We will normalize our features to fulfill this requirement. Normalization can be performed by subtracting the minimum value and dividing it by the range. Because the Landsat 8 data is a 16 bits data (216= 65536 values), the lowest and highest values are 0 and 65536. Fig. 2 also shows the result of the normalization operation.
- Reshaping the features from two to three dimensions, such that each row represents an individual pixel, is another pre-processing step. Fig. 3 indicates the result

of converting the features from two to three dimensions.

B. Architecture of the Proposed Model

In recent years, an artificial neural network (ANN) has gotten a lot of attention because of its ability to solve complicated nonlinear problems in domains like computer vision, image processing, natural language processing, and so on. For this reason, an ANN deep learning model has been implemented to improve impervious surface extraction for Marrakech, Morocco.

The basic architecture of an ANN model consists of input and output layers as well as hidden layers with various weights. Then, these several layers are connected by neurons. Every single neuron is inspired by a biological neuron, and produces a single output, and is known as a perceptron.

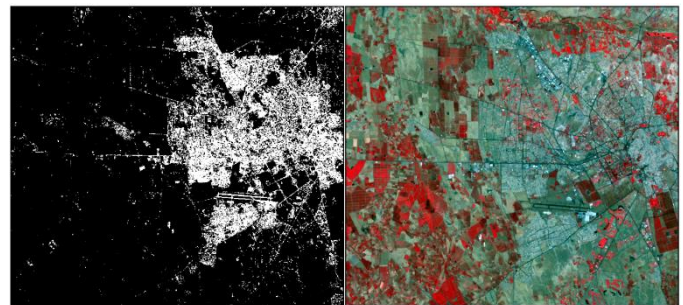


Fig. 1. Labeled Image and the Original Image.

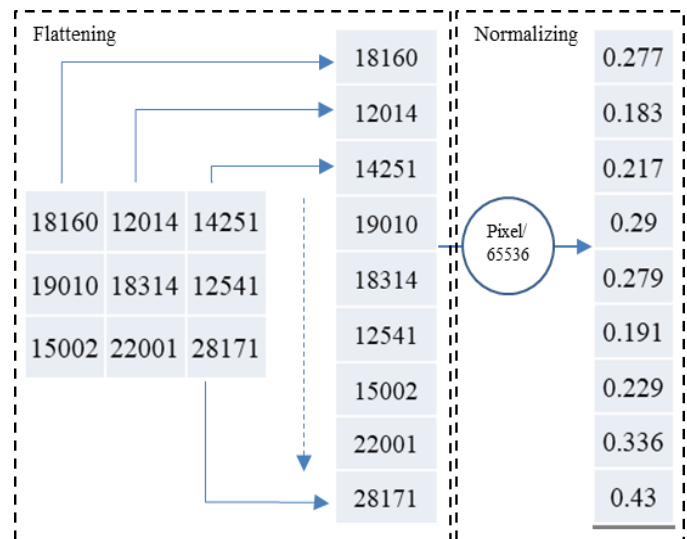


Fig. 2. Flattening and Normalizing.

B2	B3	B4	B5	B6	B7	NDVI	NDBI	Label
0.172	0
0.236	1
0.183	0
0.217	0
0.290	0
0.279	0
0.191	1
0.229	1
0.336	1
0.430	0
0.268	0

Fig. 3. Reshaping.

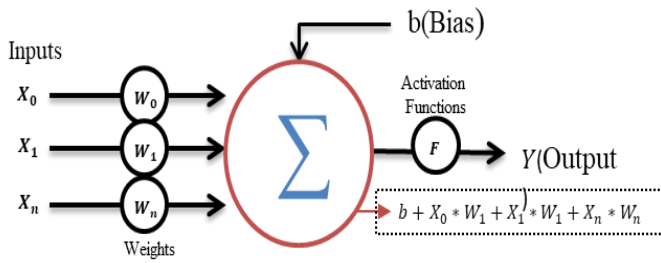


Fig. 4. Basic Architecture of ANN.

The perceptron's basic architecture is illustrated in the diagram above (Fig. 4). Initially, X_0, X_1, \dots and X_n indicate inputs. The inputs (X_0, X_1, \dots and X_n) are multiplied by a connection of weights (W_0, W_1, \dots and W_n) and then summed with the bias value b (which permits the activation function to be shifted up or down). To obtain the output of the perceptron, the output of the summation operation is applied to the activation function. If no activation function is used, the output signal is just a linear function, and the model will be unable to learn and model complex data (such as images, videos, audio, speech, and so on). A neural network needs to learn and represent anything, as well as any arbitrarily complicated function that links an input to an output. Therefore, a neural network has to use a non-linear activation function to perform this task.

C. Implementation of ANN

In our model, the input variables are Landsat 8 image bands from Band 2 – Blue to Band 7 – SWIR 2, NDVI, and NDBI. We chose the additional bands (NDVI and NDBI) to increase the amount of data, which leads to improving the performance of our model.

The proposed model has two hidden layers; the first layer contains 32 neurons, while the other contains 16 neurons, followed by an output layer with two classes, impervious and non-impervious pixels, as shown in Fig. 4. The Softmax activation function is used because it is the most suited function for our situation to estimate impervious surface pixels.

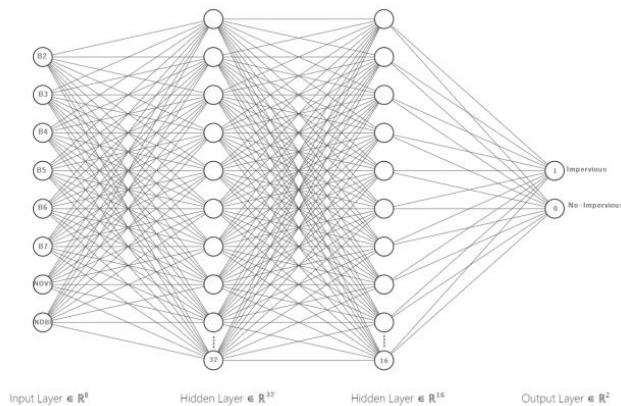


Fig. 5. Model Architecture.

IV. RESULTS AND DISCUSSION

The impervious surface classification results will be discussed in this section. To detect the impervious surfaces, a series of preprocessing steps have been implemented, as already mentioned in the previous section. We utilized an ANN model to implement the detection of impervious surfaces. This model was trained and tested using a dataset, which is taken from the Landsat-8 archive. This dataset has been corrected, filtered, and exported in the form of a Geographic Tagged Image File Format (GeoTIFF) Image (Fig. 1) in GEE. This image contains eight bands with 30 meter spatial resolution, and its dimensions are 961 pixels in height and 2476 pixels in width. To train and test the proposed model, the database is split into two parts; the first contains 60% of the database, which is used to train the model, while the other part is used for testing the model.

A. Performance Accuracy Assessment of ANN Model

At this stage, the proposed model has been implemented on the Google Colaboratory Cloud platform. This platform facilitates the training of deep learning models online by providing a lot of computing power, better than our local machines. After training and testing our model, we obtained the confusion matrix's components as shown in Table I. The explanation of the confusion matrix is as follows:

- True Positive means that the pixel is predicted as an impervious surface pixel and it's true.
- True Negative represents the pixels that are not impervious surface pixels, and it's true.
- False Positive means that the pixel is predicted as an impervious surface pixel, but it's false.
- False Negative means that the pixel is predicted as a non-impervious surface pixel, but it's false.

Table I indicated that, our model has very high performance as the positive impervious surface detection is very high and the wrong detection is low. To quantitatively evaluate our model performance, four measurements are utilized, namely accuracy, recall, precision, and F1-score.

Accuracy: The discernment required to distinguish between impervious and non-impervious surfaces. The percentage of all assessed instances that are true positive and true negative is derived to assess a test's accuracy. It can be expressed mathematically as:

$$\text{Accuracy} = \frac{(TN + TP)}{(TN + TP + FN + FP)}$$

TABLE I. THE OBTAINED RESULTS OF OUR MODEL

confusion matrix		
Output -predictable image	Actually Positive(1)	Actually Negative(0)
Impervious surface Class - 1	True positive (TP) 916106	False positive (FP) 6778
Non-Impervious surface class -0	False negative (FN) 3873	True negative (TN) 25018

That is the total number of assessments divided by the number of correct assessments. Additionally, precision, recall, and F1 score are used to assess the proposed methodology of performance. Precision is defined as the proportion of accurately predicted positive observations to all positive observations. A low proportion of false positives is associated with high precision. It can be expressed as follows:

$$\text{Precision} = \frac{TP}{TP + FP}$$

Recall: The recall is the proportion of correctly foreseen positive observations to all of the actual class observations. To put it another way, it can be expressed as.

$$\text{Recall} = \frac{TP}{TP + FN}$$

F1 Score: This is the recall and precision weighted average. As a result, both false positive and false negative numbers are taken into account. In situations where the distribution class is unbalanced, F1 is more helpful than accuracy. The formula for this is F1.

$$\text{F1 Score} = \frac{2(\text{Recall} * \text{Precision})}{(\text{Recall} + \text{Precision})}$$

Table II shows the obtained results of the four measurement parameters that have been chosen.

TABLE II. THE OBTAINED RESULTS OF THE FOUR MEASUREMENTS STATISTICAL

Accuracy	Precision	Recall	F1 Score
0.98%	0.79%	0.87%	0.82%

It can be noted from Table II that our method has high performance in all measurement parameters (accuracy, precision, recall, and F1-score) as their values are higher than 0.79%. This is because of the good design of our model architecture and the large amount of data that is used for training and testing our model.

The evaluation of our ANN model has been applied to a dataset subset covering 124 km on the western side of Marrakesh city, and its dimensions are 589 pixels in height and 1104 pixels in width. Fig. 5 shows the original image of the target area. Fig. 6 presents the output predicted image of our ANN model. Fig. 7 presents the high-resolution image from Sentinel-2 for the same area as the impervious surfaces are clearly monitored. It is noted in Fig. 6 that the impervious surfaces are represented by white pixels. In comparison with Fig. 7, we notice that the impervious surfaces are classified and detected well. Our ANN model has a high accuracy in detecting impervious surfaces.

To assess and analyze the benefits and drawbacks of the suggested model and obtain a comprehensive overview of our research region, high-resolution images from Sentinel-2 have been brought, with true color composited. Fig. 8 displays this image, which describes urbanized Lands located at the end and fringes of the city, the western side of the image, and some settlements in the south of the image.

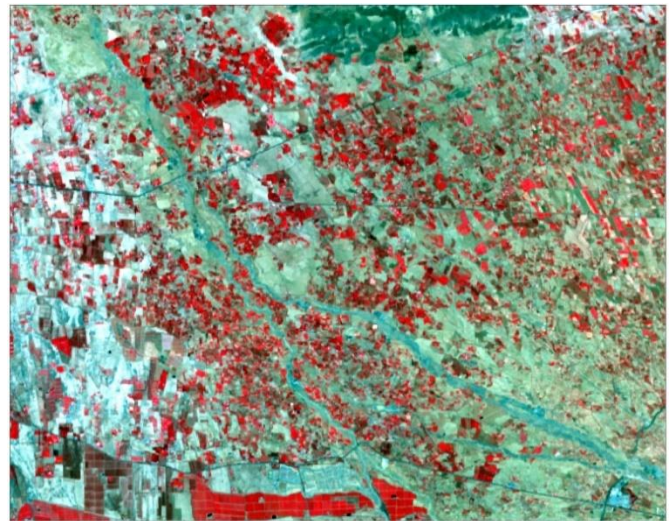


Fig. 6. Marrakech Original Image with Near-Infrared (NIR) Composite Landsat.

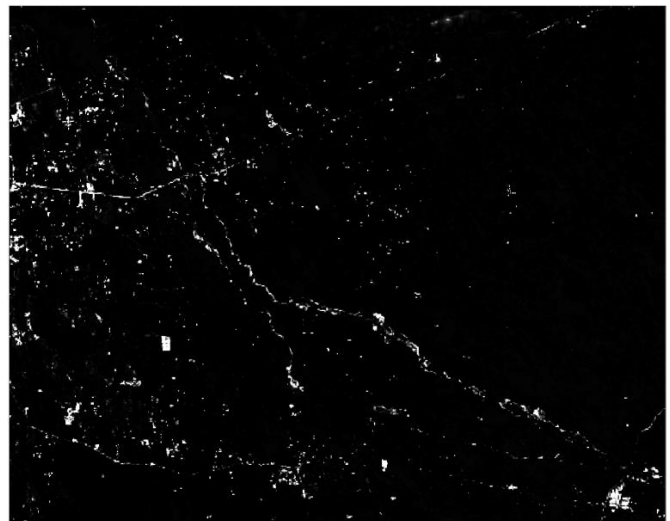


Fig. 7. Output - Predicted Image.



Fig. 8. Subset from Sentinel-2 Image for the Same Area.

V. CONCLUSION

In this paper, an artificial neural network deep learning model has been used to predict impervious surfaces in Marrakech city; the model is trained and tested using Landsat images. The experimental results show that our model has an accuracy of 81.80% in the precision matrix and 83% in the recall. This is because of the good design of our model architecture and the large amount of data that is used for training and testing our model. In the future, our goal might be to extend the proposed model to a large database containing many cities over many years. Therefore, increasing the amount of data will improve the accuracy of the model.

REFERENCES

- [1] E. B. De Colstoun et al., "Documentation for the global man-made impervious surface (GMIS) dataset from landsat," 2017.
- [2] P. Kang, W. Chen, Y. Hou, and Y. J. S. r. Li, "Spatial-temporal risk assessment of urbanization impacts on ecosystem services based on pressure-status-response framework," vol. 9, no. 1, pp. 1-11, 2019.
- [3] R. Xu, J. Liu, and J. J. S. Xu, "Extraction of high-precision urban impervious surfaces from sentinel-2 multispectral imagery via modified linear spectral mixture analysis," vol. 18, no. 9, p. 2873, 2018.
- [4] M. I. H. Reza and S. A. J. E. i. Abdullah, "Regional Index of Ecological Integrity: A need for sustainable management of natural resources," vol. 11, no. 2, pp. 220-229, 2011.
- [5] C. Liu et al., "Arctic's man-made impervious surfaces expanded by over two-thirds in the 21st century," 2022.
- [6] C. Liu et al., "An efficient approach to capture continuous impervious surface dynamics using spatial-temporal rules and dense Landsat time series stacks," vol. 229, pp. 114-132, 2019.
- [7] M. Feng and X. J. S. B. Li, "Land cover mapping toward finer scales," vol. 65, no. 19, pp. 1604-1606, 2020.
- [8] W. Kuang et al., "Global observation of urban expansion and land-cover dynamics using satellite big-data," 2021.
- [9] K. N. Markert et al., "Comparing Sentinel-1 Surface Water Mapping Algorithms and Radiometric Terrain Correction Processing in Southeast Asia Utilizing Google Earth Engine," vol. 12, no. 15, p. 2469, 2020.
- [10] A. Poortinga et al., "Predictive Analytics for Identifying Land Cover Change Hotspots in the Mekong Region," vol. 12, no. 9, p. 1472, 2020.
- [11] K. Phongsapan et al., "Operational Flood Risk Index Mapping for Disaster Risk Reduction Using Earth Observations and Cloud Computing Technologies: A Case Study on Myanmar," (in English), Original Research vol. 7, 2019-December-11 2019.
- [12] A. Poortinga et al., "An Operational Before-After-Control-Impact (BACI) Designed Platform for Vegetation Monitoring at Planetary Scale," vol. 10, no. 5, p. 760, 2018.
- [13] E. T. Slonecker, D. B. Jennings, and D. Garofalo, "Remote sensing of impervious surfaces: A review," Remote Sensing Reviews, vol. 20, no. 3, pp. 227-255, 2001/08/01 2001.
- [14] N. Khanal et al., "A Comparison of Three Temporal Smoothing Algorithms to Improve Land Cover Classification: A Case Study from NEPAL," vol. 12, no. 18, p. 2888, 2020.
- [15] Y. Wang and M. Li, "Urban Impervious Surface Detection From Remote Sensing Images: A review of the methods and challenges," IEEE Geoscience and Remote Sensing Magazine, vol. 7, no. 3, pp. 64-93, 2019.
- [16] Z. Liu, Y. Wang, and J. J. P. i. G. Peng, "Remote sensing of impervious surface and its applications: a review," vol. 29, no. 9, pp. 1143-1152, 2010.
- [17] H. Zhang, H. Lin, Y. Zhang, and Q. Weng, Remote sensing of impervious surfaces in tropical and subtropical areas. CRC Press, 2015.
- [18] M. E. Bauer, N. J. Heinert, J. K. Doyle, and F. Yuan, "Impervious surface mapping and change monitoring using Landsat remote sensing," in ASPRS annual conference proceedings, 2004, vol. 10: American Society for Photogrammetry and Remote Sensing Bethesda, MD, USA.
- [19] S. Mahyoub, H. Rhinane, M. Mansour, and A. Al Sabri, "The Use of Deep Learning in Remote Sensing for Mapping Impervious Surface: a Review Paper," in International conference of Moroccan Geomatics (Morgeo), 2020.
- [20] L. Ma, Y. Liu, X. Zhang, Y. Ye, G. Yin, and B. A. Johnson, "Deep learning in remote sensing applications: A meta-analysis and review," ISPRS Journal of Photogrammetry and Remote Sensing, vol. 152, pp. 166-177, 2019/06/01/ 2019.
- [21] L. Luo, P. Li, and X. Yan, "Deep Learning-Based Building Extraction from Remote Sensing Images: A Comprehensive Review," vol. 14, no. 23, p. 7982, 2021.
- [22] Y. Zha, J. Gao, and S. Ni, "Use of normalized difference built-up index in automatically mapping urban areas from TM imagery," International Journal of Remote Sensing, vol. 24, no. 3, pp. 583-594, 2003/01/01 2003.
- [23] H. J. P. E. Xu and R. Sensing, "Analysis of impervious surface and its impact on urban heat environment using the normalized difference impervious surface index (NDISI)," vol. 76, no. 5, pp. 557-565, 2010.
- [24] C. Liu, Z. Shao, M. Chen, and H. Luo, "MNDISI: a multi-source composition index for impervious surface area estimation at the individual city scale," Remote Sensing Letters, vol. 4, no. 8, pp. 803-812, 2013/08/01 2013.
- [25] Y. Tian, H. Chen, Q. Song, and K. Zheng, "A Novel Index for Impervious Surface Area Mapping: Development and Validation," vol. 10, no. 10, p. 1521, 2018.
- [26] C. Deng and C. Wu, "BCI: A biophysical composition index for remote sensing of urban environments," Remote Sensing of Environment, vol. 127, pp. 247-259, 2012/12/01/ 2012.
- [27] Y. Zhang, H. Zhang, and H. Lin, "Improving the impervious surface estimation with combined use of optical and SAR remote sensing images," Remote Sensing of Environment, vol. 141, pp. 155-167, 2014/02/05/ 2014.
- [28] L. Shi et al., "Impervious Surface Change Mapping with an Uncertainty-Based Spatial-Temporal Consistency Model: A Case Study in Wuhan City Using Landsat Time-Series Datasets from 1987 to 2016," vol. 9, no. 11, p. 1148, 2017.
- [29] J. Wang, Z. Wu, C. Wu, Z. Cao, W. Fan, and P. Tarolli, "Improving impervious surface estimation: an integrated method of classification and regression trees (CART) and linear spectral mixture analysis (LSMA) based on error analysis," GIScience & Remote Sensing, vol. 55, no. 4, pp. 583-603, 2018/07/04 2018.
- [30] S. Mahyoub, H. Rhinane, A. Fadil, M. Mansour, M. Saleh, and F. Al-Nahmi, "Using of Open Access remote sensing Data in Google earth engine platform for mapping built-up area in Marrakech City, Morocco. 2020, pp. 1-5.
- [31] Y. J. F. Bengio and t. i. M. Learning, "Learning deep architectures for AI," vol. 2, no. 1, pp. 1-127, 2009.
- [32] L. Zhang, L. Zhang, and B. Du, "Deep Learning for Remote Sensing Data: A Technical Tutorial on the State of the Art," IEEE Geoscience and Remote Sensing Magazine, vol. 4, no. 2, pp. 22-40, 2016.
- [33] X. X. Zhu et al., "Deep Learning in Remote Sensing: A Comprehensive Review and List of Resources," IEEE Geoscience and Remote Sensing Magazine, vol. 5, no. 4, pp. 8-36, 2017.
- [34] N. Gorelick, M. Hancher, M. Dixon, S. Ilyushchenko, D. Thau, and R. J. R. s. o. E. Moore, "Google Earth Engine: Planetary-scale geospatial analysis for everyone," vol. 202, pp. 18-27, 2017.
- [35] P. Teluguntla et al., "A 30-m landsat-derived cropland extent product of Australia and China using random forest machine learning algorithm on Google Earth Engine cloud computing platform," ISPRS Journal of Photogrammetry and Remote Sensing, vol. 144, pp. 325-340, 2018/10/01/ 2018.
- [36] F. Huang, Y. Yu, T. J. J. o. V. C. Feng, and I. Representation, "Automatic extraction of impervious surfaces from high resolution remote sensing images based on deep learning," vol. 58, pp. 453-461, 2019.
- [37] M. A. Wulder et al., "The global Landsat archive: Status, consolidation, and direction," Remote Sensing of Environment, vol. 185, pp. 271-283, 2016/11/01/ 2016.

- [38] M. A. Wulder, J. G. Masek, W. B. Cohen, T. R. Loveland, and C. E. Woodcock, "Opening the archive: How free data has enabled the science and monitoring promise of Landsat," *Remote Sensing of Environment*, vol. 122, pp. 2-10, 2012/07/01/ 2012.
- [39] C. Deng and C. J. R. S. o. E. Wu, "A spatially adaptive spectral mixture analysis for mapping subpixel urban impervious surface distribution," vol. 133, pp. 62-70, 2013.
- [40] W.-z. Yue and C.-f. J. J. O. R. S.-B.-. Wu, "Urban impervious surface distribution estimation by spectral mixture analysis," vol. 11, no. 6, p. 914, 2007.
- [41] X. Zhang and S. Du, "A Linear Dirichlet Mixture Model for decomposing scenes: Application to analyzing urban functional zonings," *Remote Sensing of Environment*, vol. 169, pp. 37-49, 2015/11/01/ 2015.
- [42] H. Ko, S. B. Hofer, B. Pichler, K. A. Buchanan, P. J. Sjöström, and T. D. J. N. Mrcic-Flogel, "Functional specificity of local synaptic connections in neocortical networks," vol. 473, no. 7345, pp. 87-91, 2011.
- [43] M. Zhou, R. Zhang, W. Xie, W. Qian, and A. Zhou, "Security and Privacy in Cloud Computing: A Survey," in 2010 Sixth International Conference on Semantics, Knowledge and Grids, 2010, pp. 105-112.
- [44] M. Al-Ruithe, E. Benkhelifa, K. J. P. Hameed, and U. Computing, "A systematic literature review of data governance and cloud data governance," vol. 23, no. 5, pp. 839-859, 2019.
- [45] M. Belgiu, L. J. I. j. o. p. Drăguț, and r. sensing, "Random forest in remote sensing: A review of applications and future directions," vol. 114, pp. 24-31, 2016.
- [46] S. Piramanayagam, W. Schwartzkopf, F. Koehler, and E. Saber, "Classification of remote sensed images using random forests and deep learning framework," in *Image and signal processing for remote sensing XXII*, 2016, vol. 10004, pp. 205-212: SPIE.